DOI:
10.1088/1361-6463/aaf260

Document Version
Peer reviewed version

Improving propagation lengths of ultraviolet surface plasmon polaritons on thin aluminium films by ion milling.

W. P. Wardley, F. J. Rodríguez-Fortuño, A. V. Zayats, W. Dickson

Department of Physics, King's College London, Strand, London WC2R 2LS, United Kingdom

Abstract

Ultraviolet (UV) plasmonics provides several benefits over the visible or infrared spectral range. The intrinsic optical properties of aluminium make it the best material for ultraviolet-based plasmonic systems, but in practice thin aluminium films exhibit higher roughnesses than those of other metals grown by physical vapour deposition. This roughness increases scattering losses, decreasing surface plasmon polariton propagation length. Here we experimentally demonstrate a method for improving the optical quality of aluminium films using an ion milling post-deposition processing step to reduce surface roughness. The propagation length of surface plasmon polaritons (SPPs) has been measured in the ultraviolet spectral range using grating pairs fabricated by focused ion beam milling. The propagation length for as-deposited films has been compared with films produced by normal incidence and oblique angle milling. An increase in propagation length of about 20% was observed for both normal and oblique angle milling.

Surface plasmon polaritons (SPPs), collective oscillations of free electrons coupled to the electric field of incident light that propagate along the surface of a dielectric-conductor interface, demonstrate high field confinement and high sensitivity to changes to the refractive index of their environment. As a result, they have been mooted as a useful tool in a number of scenarios, including optical circuitry, due to their high field confinement [1-5] and as sensors and detectors, due to their high environmental sensitivity [6-11]. A number of different sensors already exist both at the research and development stage [12, 13] and also as extant technology, such as in SPR sensors [7, 9], but the spectral window of these devices has been limited to the visible or longer wavelengths.

Ultraviolet plasmonics features a number of benefits over the visible or infrared spectral range. The autofluorescence of biological molecules typically lies in the UV, for instance DNA will fluoresce at around 340 nm, which can be enhanced by coupling to plasmonic systems [14]. Surface Enhanced Raman Spectroscopy (SERS) systems will also benefit from UV wavelength range; SERS enhancement scales to ω^4, allowing for significant gains in the UV [15-18]. In order to achieve UV plasmonics, sensible material choices have to be made. Most plasmonic studies to date have relied on the coinage metals, Au, Ag, Cu, etc., but due to high inter- and intraband losses these materials become very poor supporters of SPPs in the UV. There are a number of other metals that have appropriate complex permittivity (e.g. Rh, Mg, Pt, Pd), but the most effective is aluminium [19-21], with the largest real part and smallest imaginary permittivity components in the UV spectral range.

While aluminium is theoretically the best material choice for thin-film plasmonics in the ultraviolet, it does present a number of drawbacks. It is well known, for instance, that thin aluminium films show higher roughnesses than equivalent films of other metals grown by the same method, due to electromigration effects, internal stresses and the presence of trace amounts of oxygen, which react with the aluminium to form oxides [22-24].

SPP quality can be quantified in a number of ways; the method presented below will focus on the SPP propagation length. This is defined as the distance along conductor/insulator interface at which the SPP intensity has decayed by a factor of 1/e [25]. The propagation length of an SPP is related to a number of parameters; the materials making up the interface, the wavelength of illumination, but also the physical properties of the interface [26, 27]. For instance, surface roughness will decrease the propagation length due to scattering, which will allow the SPP to decay into an emitted photon [28]. This means in order to produce SPP-utilising systems for broader applications it is important to try to produce metal films with the lowest roughness possible.

SPPs can be generated in a number of ways [28], but due to a momentum mismatch cannot be produced by simple illumination of a metal surface. This mismatch can be overcome by using a prism coupling system, scattering from surface objects, excitation in the near-field, such as from a SNOM probe, or by use of a grating, or plasmonic crystal; nanostructured gratings designed to allow the coupling of light into SPPs at specific wavelengths and incidence angles [29, 30]. The period of the grating can be calculated, for a metal-air interface and assuming that the grating lattice vector is contained in the plane of incidence, via the following momentum matching condition [28]:

$$k_0 \sin\theta = \underbrace{k_0\sqrt{\frac{\varepsilon}{1+\varepsilon}}}_{k_{\mathrm{SPP}}} + m\underbrace{\frac{2\pi}{D}}_{k_g} \tag{1}$$

where $k_0 = 2\pi/\lambda$ is the wave-number, θ is the angle of incidence, ε is the relative permittivity of the metal, m is an integer, D is the spacing between grating elements, k_{SPP} is the SPP propagation constant, and k_g is the grating wave-vector.

There are a number of different approaches available to reduce the roughness of the sputtered aluminium film; including as-sputtering techniques such as varying the sputter rate, the substrate temperature and the sputtering gas composition and pressure[31-34], and post-processing techniques such as film annealing[35] film lift-off from a pre-patterned silicon wafer [36] or pre-doping the substrate surface with a nucleating seed layer [37, 38]. However, all of these post-deposition methods require the addition of another material, epoxy in the case of film lift-off and either metallic or polymer nucleating agents in the seeding process, which will typically have a significant and negative impact on the UV optical properties of the final film.

In this work, we present a method for improving the SPP propagation length on aluminium films via a reduction in surface roughness from an ion milling step in the film production process. As SPPs propagate across a metal surface, roughness centres will act as point scatterers, allowing radiative losses (Fig 1a), so by reducing roughness there should be fewer losses and therefore greater SPP propagation length. Two different milling approaches will be taken, normal incidence (Fig. 1c) and high angle milling (Fig. 1d), which will be compared to an otherwise identical as-sputtered film (Fig 1b).

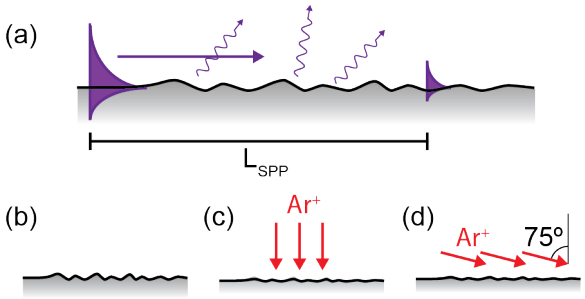

FIG. 1. (a) Surface roughness enables radiative losses of the SPP, reducing its propagation length. (b) Sputtered aluminium film. (c) Aluminium film ion milled at normal incidence. (d) Aluminium film under high angle ion milling.

The aluminium films were produced by sputter depositing a 50 nm film in a Kurt J Lesker PVD75 using conditions previously calibrated to produce low roughnesses (300W DC power, 3 mTorr chamber argon pressure). The samples to be ion milled were then placed in an SVS6000 fitted with an argon ion gun. One sample was milled at normal incidence for 30 minutes using a low beam power (10 mA/cm^2 beam current, 390 V acceleration voltage) and another at 75° for 3 minutes using a mid-power beam (23 mA/cm^2 beam current, 1 kV acceleration voltage) known to mill samples without significantly ablating excess material. The beam powers, durations and angles of incidence were all predetermined via production of a series of calibration samples, with particular focus paid to reducing the surface roughness to the maximum extent without significantly reducing the film thickness. When identical beam powers were used to attempt to standardise the procedure, we found that there was no noticeable change on the angled sample with the low beam power, via AFM roughness measurement, whereas the normal incidence film was destroyed by the higher power beam, even for the shorter exposure time.

To measure the propagation length of SPPs on the different aluminium films, plasmonic crystals were used as a means of in-coupling and out-coupling SPPs to the aluminium-air interface. The incident laser beam couples into an SPP via the in-coupling grating. The SPP then propagates along the aluminium-air interface for a distance d, during which it decays, and then reaches a second grating where it out-couples (see Fig. 2(a)). Both line gratings were produced by gallium FIB milling of lines in the surface of the film. Pairs of gratings with different periods were chosen, to allow different in-coupling and out-coupling angles. This different coupling angle allowed the removal of any transmitted laser power that would saturate our measurements, by illuminating the in-coupling grating at a larger angle than the collection angle of the objective lens, as determined by the NA. As a 50x Mitutoyo UV M Plan lens was used with a 0.4NA, which corresponds to a collection half-angle of 23.5°, an illumination angle of $\theta = 30°$ was selected. The illumination source was a 375 nm Horiba delta diode laser. The grating parameters were calculated via equation (1), with the m=-1 grating mode allowing coupling to and from the aluminium-air SPP at the desired angles, giving a 714nm period for 30° in-coupling and a 366 nm period for normal incidence out-coupling. The gratings were further characterised by AFM, shown in Fig. 2(b). This also allowed a direct measurement of surface roughness, with the measurements taken in the inter-grating region through which the SPPs propagate.

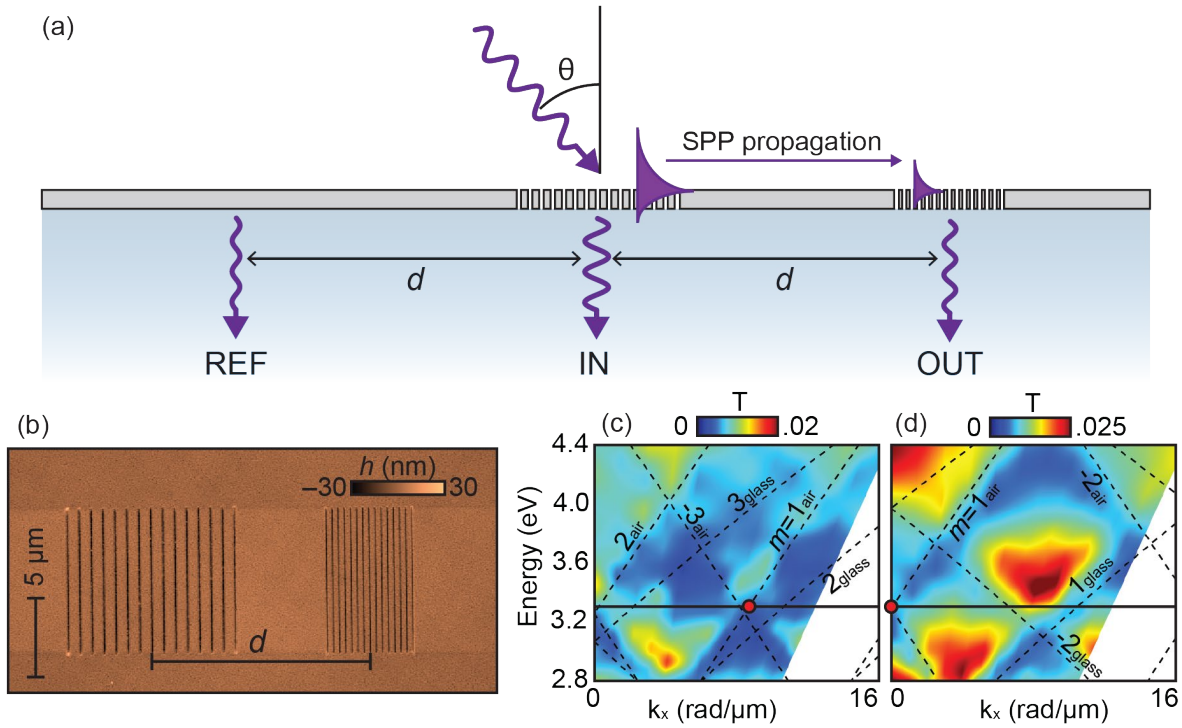

FIG. 2. (a) Schematic diagram of the measurement setup showing the illumination of gratings along with the location of the 3 measurement sites, on the incoming grating (IN), on the out-coupling grating (OUT) and a distance d in the opposite direction from the in-coupling grating (REF). (b) AFM image of the two gratings (c,d) transmission dispersion diagrams of the two gratings, with the expected theoretical dispersion relations (Eq. 1) superimposed as dashed lines for different values of the grating order *m*. The 30° incidence in (b) and the 0° normal incidence in (d) for which the gratings were designed to work at 375nm (3.31 eV) are marked as a red dot, overlapping with the m=1 dispersion relation of the aluminium-air interface.

In order to confirm the coupling behaviour of the gratings, transmission spectra measurements of both gratings were taken at varying angles, allowing the plotting of the grating dispersions, shown in Fig. 2(c). These confirmed the presence of suitable coupling behaviour of incident light to aluminium-air SPPs at 375nm (3.31 eV) at the corresponding angles.

To measure the propagation length across the films, different samples with varying separation distances between the gratings were used. As centre-to-centre distances are used as the measure of separation, the smallest separation distance (without gratings overlapping) was 12 μm, with separations increasing in 2 μm steps up to 22 μm. Propagation lengths were measured by illuminating the in-coupling grating at 375nm at a constant power. By measuring the out-coupled light at three sites, the out-coupling grating [labelled as I_{out} in Fig. 1(a)], the in-coupling grating [labelled as I_{in}] and a point on the film at a distance equal to the grating separation on the opposite side of the in-coupling grating [labelled as I_{ref}], as shown in Fig. 2(a), we obtained signal, reference and background measurements accordingly. The linearity of Maxwell's equations ensures that the power of the SPP wave launched by the in-coupling grating will be linearly proportional to the I_{in} measurement, while the power of the SPP reaching the out-coupling grating after decay will be linearly related to the I_{out} measurement. The proportionality constants of both can be arbitrary.

To calculate the propagation length L_{SPP} from the intensity decay of the SPP after propagating a distance *d*, we use the definition of propagation length[28]:

$$\ln\left(\frac{I_{\mathrm{out}}}{I_{\mathrm{in}}}\right) = \left(\frac{-1}{L_{\mathrm{SPP}}}\right) d + C \tag{2}$$

Where I_{in} and I_{out} would ideally correspond to the SPP intensity before and after propagation. In practice, we use I_{in} and I_{out} as the intensities that are scattering from the in-coupling and out-coupling gratings into our objective after subtraction of the background measurement I_{ref}. The gratings scatter in all directions, and our objective collects the total scattering in a certain angular range. The important thing to realise is that the collected scattering intensity from each grating will be linearly proportional to the corresponding SPP intensities, with a proportionality constant that is unknown and depends on many factors, but is accounted for by the arbitrary constant C. The measured data is shown in Fig. 3(b). The gradient of the straight-line fit here provides the propagation length. The propagation lengths for the SPPs were found to be 4.26 (±0.92) µm for the unmilled film, 5.13 (±0.87) µm for the normal incidence milled film and 5.24 (±0.60) µm for the 75° milled film.

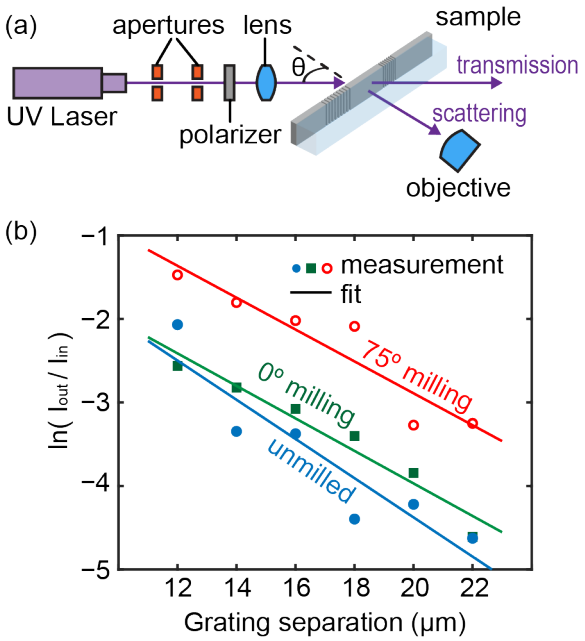

Fig. 3. (a) Experimental apparatus and (b) transmitted power measurements for different Al films. Lines of best fit and associated uncertainties were calculated using least squared error.

It is possible to calculate the maximum propagation length for the ideal case of perfectly smooth aluminium by using [25]

$$L_{\mathrm{SPP}} = \frac{1}{2\,\mathrm{Im}(k_{SPP})} \tag{3}$$

where k_{SPP} is defined in Eq. (1). Inserting the relevant permittivity of aluminium from tabulated data[39], which is -20.29 + 3.831i at 375 nm wavelength, allows calculation of the maximum propagation length for films on ideal, smooth aluminium of 6.18 μm.

The effect of roughness will be to reduce this propagation length, and this can be accounted for from a theoretical point of view [40-42]. The propagation constant for SPPs, corrected for roughness, can be written as a correction term added to the ideal smooth interface case $k_{\mathrm{SPP}}^{r} = k_{\mathrm{SPP}} + \Delta k$, where the correction term Δk can be calculated by applying Eq. (A42) in Ref. [40]. Inserting the modified k_{SPP}^{r} into Eq. (3) gives us a theoretical estimation of the reduced propagation length due to roughness. The calculation of Δk assumes a metal-air interface in which the roughness correlation function is modelled as isotropic and Gaussian, defined by only two roughness parameters: the correlation length σ, and the root mean square height of the roughness δ. Specifically, given a height topography map for the surface of our sample $h(\mathbf{r})$, with $\mathbf{r} = (x, y)$, we can calculate the correlation function of the roughness and approximate it to a Gaussian function as:

$$G(\mathbf{\Delta r}) = \frac{1}{S}\iint_{S} h(\mathbf{r})h(\mathbf{r}+\mathbf{\Delta r})\, d\mathbf{r} \approx \delta^2 \exp\left(-\frac{|\mathbf{\Delta r}|^2}{\sigma^2}\right) \qquad (4)$$

where S is a given surface under analysis. From AFM measurements of $h(\mathbf{r})$ (Fig 4(a-c)) we made the corresponding Gaussian least squared error fits (Fig. 4(d)) following Eq. (4). The roughness parameters (δ, σ) and theoretical calculation of propagation lengths expected for each roughness is given in Table 1, together with the propagation lengths experimentally observed from the power measurements in Fig. 3.

Table 1: Roughness amplitude, roughness correlation distances and SPP propagation lengths calculated from AFM analysis compared with optical measurements

	Unsmoothed	**Smoothed 0°**	**Smoothed 75°**
Roughness RMS amplitude δ (nm)	3.4	2.5	2.9
Roughness correlation distance σ (nm)	29.0	35.2	29.7
Theoretical SPP propagation length L_{SPP}^{r} (μm)	3.88	4.91	4.36
Measured SPP propagation length L_{SPP}^{meas} (μm)	4.26 ± 0.92	5.13 ± 0.87	5.24 ± 0.60

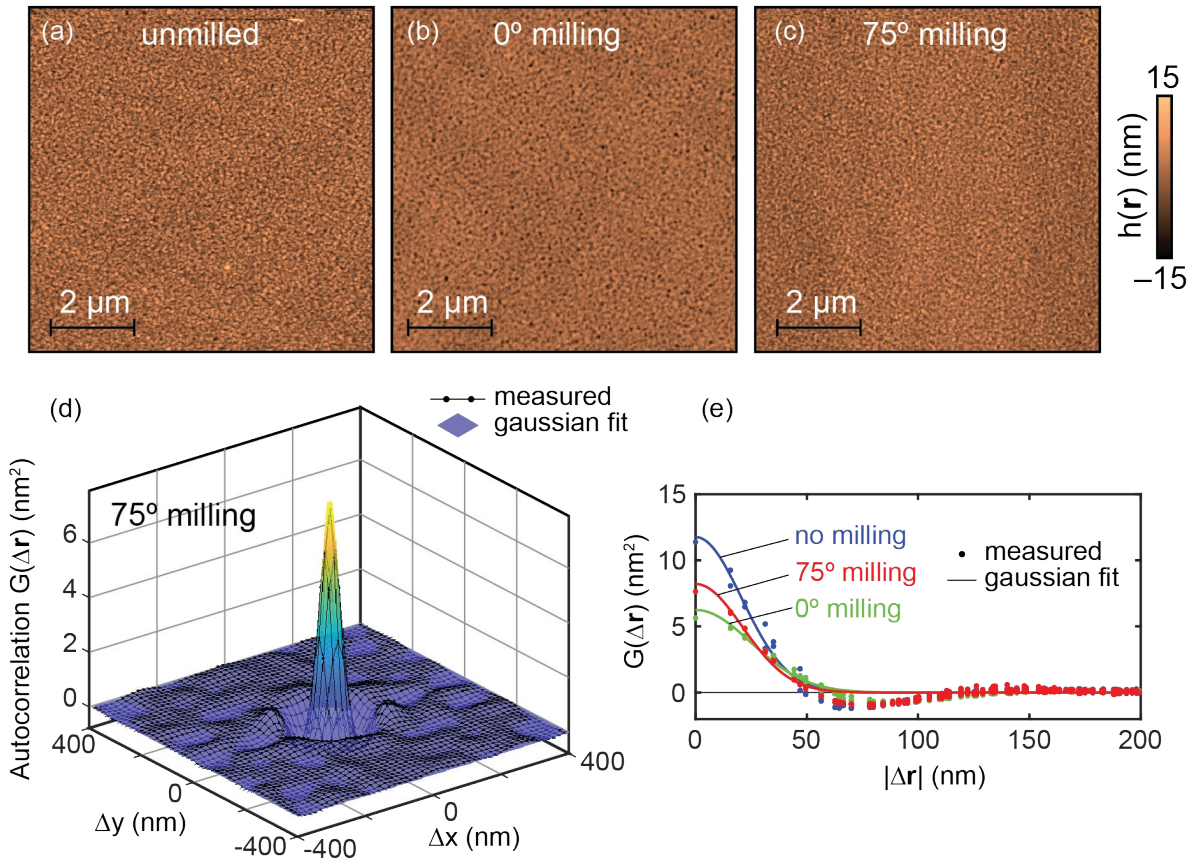

Fig. 4. AFM topography of the three aluminium surfaces (a) unmilled, (b) 0° milled and (c) 75° milled. (d) 2D correlation function corresponding to the image (c) fitted with a Gaussian. (e) 2D correlation function for the three measurements (a-c), projected into the radial displacement variable.

On inspection of Table 1 and Figure 4, it can be clearly observed that the milling process has reduced the surface roughness measured using AFM, with an associated increase in propagation length. The measured propagation lengths from the optical measurements lie within the theoretical calculations, within errors, for the unsmoothed and 0 degrees smoothed films. The theoretical estimations consistently overestimate the effects of roughness, as is typically the case, due to the theoretical approximations and assumptions [41].

The use of an ion milling post-deposition fabrication step can measurably reduce roughness on sputtered thin film aluminium. This also measurably increases the propagation length of SPPs on these metal films. This is demonstrated here by measurement of UV SPPs on thin aluminium films produced by sputter deposition and then ion milled at both normal incidence and high angle, both of which produced a significant (>20%) increase in SPP propagation length. The trend in propagation length increase is also compared to theoretically derived values calculated from AFM images of the thin film surfaces. This offers a simple, cheap technique using technology frequently found integrated in sputtering systems to routinely produce higher quality aluminium films than as-sputtered, therefore increasing the propagation length of UV surface plasmon polaritons on aluminium-based nanophotonic devices.

Acknowledgements

This work has been supported in part by the EPSRC (UK). A Z acknowledges support from the Royal Society and the Wolfson Foundation. FJRF acknowledges support from European Research Council project ERC-2016-STG-714151-PSINFONI.

References

1. Bozhevolnyi, S.I., *Plasmonic Nano-Guides and Circuits.* Frontiers in Optics 2008/Laser Science XXIV/Plasmonics and Metamaterials/Optical Fabrication and Testing (2008), paper MWD3, 2008.
2. Fang, Y. and M. Sun, *Nanoplasmonic waveguides: towards applications in integrated nanophotonic circuits.* Light: Science & Applications, 2015. **4**(6).
3. Boltasseva, A., et al., *Integrated Optical Components Utilizing Long-Range Surface Plasmon Polaritons.* Journal of Lightwave Technology, Vol. 23, Issue 1, pp. 413-, 2005.
4. Zayats, A.V., I.I. Smolyaninov, and A.A. Maradudin, *Nano-optics of surface plasmon polaritons.* Physics Reports, 2005. **408**(3-4): p. 131-314.
5. Krasavin, A.V., A.V. Zayats, and N.I. Zheludev, *Active control of surface plasmon–polariton waves.* Journal of Optics A: Pure and Applied Optics, 2005. **7**(2): p. S85-S89.
6. Jorgenson, R.C. and S.S. Yee, *A fiber-optic chemical sensor based on surface plasmon resonance.* Sensors and Actuators B: Chemical, 1993. **12**(3): p. 213-220.
7. Piliarik, M., L. Parova, and J. Homola, *High-throughput SPR sensor for food safety.* Biosens Bioelectron, 2009. **24**(5): p. 1399-404.
8. Willets, K.A. and R.P. Duyne, *Localized Surface Plasmon Resonance Spectroscopy and Sensing.* Annual Review of Physical Chemistry, 2007. **58**(1): p. 267-297.
9. Homola, J., et al., *Surface Plasmon Resonance (SPR) Sensors*. 2016: Springer Berlin Heidelberg. 45-67.
10. Liedberg, B., C. Nylander, and I. Lunström, *Surface plasmon resonance for gas detection and biosensing.* Sensors and Actuators, 1983. **4**: p. 299-304.
11. Brolo, A.G., et al., *Surface Plasmon Sensor Based on the Enhanced Light Transmission through Arrays of Nanoholes in Gold Films.* Langmuir, 2004. **20**(12): p. 4813-4815.
12. Kabashin, A.V., et al., *Plasmonic nanorod metamaterials for biosensing.* Nat Mater, 2009. **8**(11): p. 867-71.
13. Anker, J.N., et al., *Biosensing with plasmonic nanosensors.* Nat Mater, 2008. **7**(6): p. 442-53.
14. Lakowicz, J.R., et al., *Intrinsic fluorescence from DNA can be enhanced by metallic particles.* Biochem Biophys Res Commun, 2001. **286**(5): p. 875-9.
15. Kneipp, K., *Surface-enhanced Raman scattering.* Physics Today, 2007. **60**(11): p. 40-46.
16. Yang, Z.L., et al., *Tunable SERS from aluminium nanohole arrays in the ultraviolet region.* Chem Commun (Camb), 2011. **47**(13): p. 3909-11.
17. Sigle, D.O., et al., *Reproducible Deep-UV SERRS on Aluminum Nanovoids.* J Phys Chem Lett, 2013. **4**(9): p. 1449-52.
18. Mogensen, K.B., et al., *Surface-enhanced Raman scattering on aluminum using near infrared and visible excitation.* Chem Commun (Camb), 2014. **50**(28): p. 3744-6.
19. Gérard, D. and S.K. Gray, *Aluminium plasmonics.* Journal of Physics D: Applied Physics, 2015. **48**(18): p. 184001.
20. Knight, M.W., et al., *Aluminum for plasmonics.* ACS Nano, 2014. **8**(1): p. 834-40.
21. Chubchev, E.D., et al., *Highly confined surface plasmon polaritons in the ultraviolet region.* Opt Express, 2018. **26**(7): p. 9050-9062.
22. Bordo, K. and H.-G. Rubahn, *Effect of Deposition Rate on Structure and Surface Morphology of Thin Evaporated Al Films on Dielectrics and Semiconductors.* Materials Science, 2012. **18**(4).

23. Furukawa, M., et al., *Surface morphologies of sputter-deposited aluminum films studied using a high-resolution phase-measuring laser interferometric microscope.* Appl Opt, 1996. **35**(4): p. 701-7.
24. McPeak, K.M., et al., *Plasmonic Films Can Easily Be Better: Rules and Recipes.* ACS Photonics, 2015. **2**(3): p. 326-333.
25. Barnes, W.L., *Surface plasmon–polariton length scales: a route to sub-wavelength optics.* Journal of Optics A: Pure and Applied Optics, 2006. **8**(4): p. S87-S93.
26. Arakawa, E.T., et al., *Effect of Damping on Surface Plasmon Dispersion.* Physical Review Letters, 1973. **31**(18): p. 1127-1129.
27. Braundmeier, A.J. and E.T. Arakawa, *Effect of surface roughness on surface plasmon resonance absorption.* Journal of Physics and Chemistry of Solids, 1974. **35**(4): p. 517-520.
28. Maier, S.A., *Plasmonics: Fundamentals and Applications*. Plasmonics: Fundamentals and Applications. 2007: Springer.
29. Zayats, A.V. and I.I. Smolyaninov, *Near-field photonics: surface plasmon polaritons and localized surface plasmons.* Journal of Optics A: Pure and Applied Optics, 2003. **5**(4): p. S16-S50.
30. Iqbal, T., *Propagation length of surface plasmon polaritons excited by a 1D plasmonic grating.* Current Applied Physics, 2015. **15**(11): p. 1445-1452.
31. Chu, H.-Y., et al., *The Influence of Sputtering Power of Aluminum Film in Aluminum Induced Crystallization of Low Temperature Poly-Silicon Film.* 2006: p. 1190-1193.
32. Koski, K., J. Hölsä, and P. Juliet, *Voltage controlled reactive sputtering process for aluminium oxide thin films.* Thin Solid Films, 1998. **326**(1-2): p. 189-193.
33. Koski, K., J. Hölsä, and P. Juliet, *Properties of aluminium oxide thin films deposited by reactive magnetron sputtering.* Thin Solid Films, 1999. **339**(1-2): p. 240-248.
34. Koenig, H.R. and L.I. Maissel, *Application of RF Discharges to Sputtering.* IBM Journal of Research and Development, 1970. **14**(2): p. 168-171.
35. D'Heurle, F.M., *Aluminum Films Deposited by RF Sputtering.* Metallurgical and Materials Transactions B, 1970. **1**(3): p. 725-732.
36. Nagpal, P., et al., *Ultrasmooth patterned metals for plasmonics and metamaterials.* Science, 2009. **325**(5940): p. 594-7.
37. Liu, H., et al., *Enhanced surface plasmon resonance on a smooth silver film with a seed growth layer.* ACS Nano, 2010. **4**(6): p. 3139-46.
38. Ke, L., et al., *Ultrasmooth silver thin film on PEDOT:PSS nucleation layer for extended surface plasmon propagation.* ACS Appl Mater Interfaces, 2012. **4**(3): p. 1247-53.
39. Rakic, A.D., *Algorithm for the determination of intrinsic optical constants of metal films: application to aluminum.* Appl Opt, 1995. **34**(22): p. 4755-67.
40. Fontana, E. and R.H. Pantell, *Characterization of multilayer rough surfaces by use of surface-plasmon spectroscopy.* Physical Review B, 1988. **37**(7): p. 3164-3182.
41. Kolomenski, A., et al., *Propagation length of surface plasmons in a metal film with roughness.* Appl Opt, 2009. **48**(30): p. 5683-91.
42. Toigo, F., et al., *Optical properties of rough surfaces: General theory and the small roughness limit.* Physical Review B, 1977. **15**(12): p. 5618-5626.